

Depth Camera Based on Color-Coded Aperture

Vladimir
Paramonov
v.paramonov
@samsung.com

Ivan
Panchenko
i.panchenko
@samsung.com

Victor
Bucha
v.bucha
@samsung.com

Andrey
Drogolyub
a.drogolyub
@samsung.com

Sergey
Zagoruyko
s.zagoruyko
@samsung.com

Samsung R&D Institute Russia, Moscow, Russian Federation

Abstract

In this paper we present a single-lens single-frame passive depth sensor based on conventional imaging system with minor hardware modifications. It is based on color-coded aperture approach and has high light-efficiency which allows capturing images even with handheld devices with small cameras. The sensor measures depth in millimeters in the whole frame, in contrast to prior-art approaches. Contributions of this paper are: (1) introduction of novel light-efficient coded aperture designs and corresponding algorithm modification; (2) depth sensor calibration procedure and disparity to depth conversion method; (3) a number of color-coded aperture based depth sensor implementations including a DSLR based prototype, a smartphone based prototype and a compact camera based prototype; (4) applications including real-time 3D scene reconstruction and depth based image effects.

1. Introduction

Scene depth extraction, i.e. computation of distances to all scene points, is an important part of computational photography. There are various approaches for depth extraction: a stereo camera and a camera array in general, a plenoptic camera, a camera with coded aperture. The stereo camera is the most common solutions but it is still rarely used in smartphones due to high cost and extra space required. Other approaches use multiple images for depth extraction and work only for static scenes. Thuswise, the coded aperture approach is a promising single-lens single-frame solution which requires insignificant hardware modification ([3]) and can provide a depth quality sufficient for some applications (e.g., [2, 4]). However, a number of issues has to be solved and are discussed in this paper: (1) Light efficiency has to be increased for a handheld device; (2) Diffraction limit is close for millimeter-size lenses (e.g., smartphones) and aperture design efficiency should be ver-

ified practically; (3) To estimate real depth in millimeters one has to develop a special disparity to depth conversion method for coded aperture;

1.1. Related Work

Depth can be estimated using a camera with binary coded aperture [13, 19]. It requires computationally expensive depth extraction techniques based on multiple deconvolutions and a sparse image gradient prior. Disparity extraction using a camera with color-coded aperture which produces spatial misalignment between color channels was first demonstrated in 1992 [1] and has changed insignificantly since that time [4, 11, 12]. The main advantage of these cameras over cameras with binary coded aperture is lower computational complexity of depth extraction techniques which do not require time-consuming deconvolutions.

The light efficiency of the systems proposed in [1, 4, 11, 12, 13, 19, 22] is less than 20%, which leads to decreased Signal-to-Noise Ratio (SNR) or longer exposure times with motion blur. That makes them impractical for compact hand-held devices. A possible solution was proposed in [5], where each color channel has individual effective aperture size. Therefore, the resulting image has color channels with different depths-of-field. Due to symmetrical design this coded aperture cannot provide discrimination between objects closer or further than in-focus distance. Furthermore, it requires a time-consuming disparity extraction algorithm. We propose a solution to the problems listed above.

A simplified imaging system is illustrated schematically in Figure 1. It consists of a single thin lens and RGB color sensor. A coded aperture is placed next to the thin lens. The aperture consists of color filters with different passbands, e.g. red and green color filters (Figure 2). Defocused regions of an image captured with this system have different viewpoints in red and green color channels (see Figure 2(b)). By considering the correspondence between these two channels the disparity map for the captured scene

can be estimated as in [1].

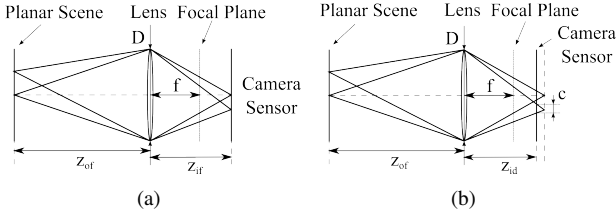


Figure 1. Conventional single lens imaging system image formation: (a) focused scene; (b) defocused scene.

The original color image cannot be restored in the case of blue channel absence. Authors of [4, 11, 12] changed the aperture design to include three color channels and enhanced the disparity map quality.

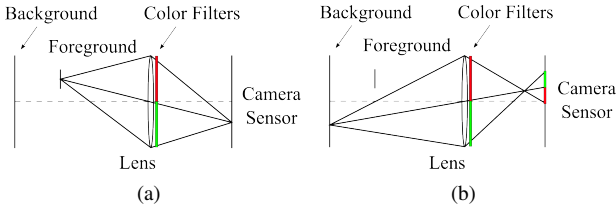


Figure 2. color-coded aperture image formation: (a) in-focus foreground; (b) defocused background.

To get the depth map from an estimated disparity map one may use the thin lens equation. In practice, most of prior art works in this area do not discriminate disparity and depth treating them as synonyms as one-to-one correspondence exists. However, a modern imaging system usually consists of a number of different lenses, i.e. an objective. The planar scene does not have plain depth if we apply trivial disparity-to-depth conversion equation. A number of researchers worked on this problem for different optics systems [7, 10, 17, 18]. Depth results (we say about depth in mm) for coded aperture cameras [16, 12] are valid only in the center of captured image.

1.2. Structure of the Paper

This paper is organized as follows: we propose light-efficient aperture designs in Section 2; in Section 3, we present a novel method of disparity to depth conversion for generalized optical system which provides a valid depth in the whole frame; we make an evaluation of our work in Section 4 and show the prototypes and implementations (including 3D reconstruction using coded aperture based depth sensor) in Section 5.

2. Color-Coded Aperture

2.1. Aperture Designs

We implemented a number of light-efficient aperture designs in Figure 3. In contrast to prior-art designs, we used sub-apertures of complementary colors and non-congruent shapes.

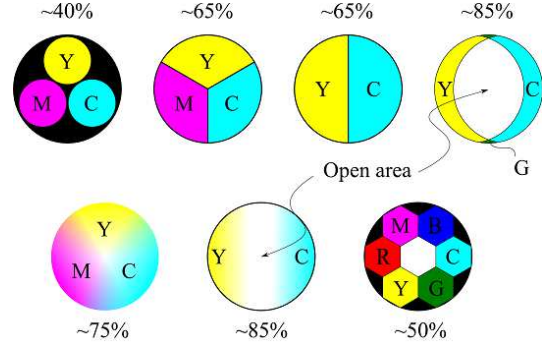


Figure 3. Possible color-coded aperture designs with corresponding light efficiency approximation (based on effective area sizes).

Let us consider the semi-circles aperture design illustrated in Figure 3. It consists of yellow and cyan filters. The yellow color filter has a passband which includes green and red light passbands. The cyan color filter has a passband which includes green and blue light passbands. The green channel is not distorted by those filters and can be used as a reference in the image restoration procedure. With ideal filters this design has a light efficiency over 65% with respect to a fully open aperture.

2.2. Color Space Change

An image is captured in sensor color space, e.g. RGB. However, the disparity estimation algorithm works in coded aperture color space, e.g. CYX, shown in Figure 4(a).

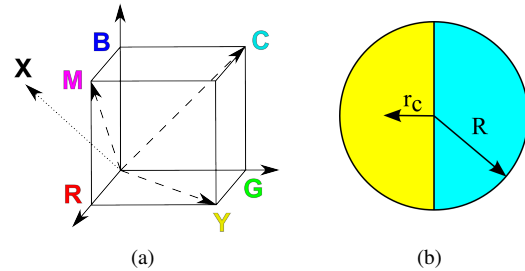


Figure 4. (a) CYX color space visualization: C - cyan, Y - yellow and X is a vector orthogonal to the CY plane. (b) Cyan and yellow coded aperture dimensions.

To translate the image from RGB to CYX color space, a transform matrix \mathbf{M} is estimated similar to [1]. Then, for each pixel of the image we have:

$$\mathbf{w}_{CYX}^{i,j} = \mathbf{M}^{-1} \mathbf{w}_{RGB}^{i,j}, \quad (1)$$

where $\mathbf{w}_{CYX}^{i,j}$ and $\mathbf{w}_{RGB}^{i,j}$ are vectors representing the color of the (i,j) pixel in CYX and RGB color spaces respectively.

3. Depth Map Estimation

In this section we describe a novel method of depth computation for coded aperture cameras in the whole frame.

3.1. Disparity Map Estimation

For disparity map estimation we used the algorithm proposed in [16]. It computes a mutual correlation of color channels in exponentially weighted window and uses bilateral filter approximation for cost volume regularization. In contrast to the original work [16], we applied this algorithm not in sensor color space but in color-coded aperture color space. This increases texture correlation between color channels if they have overlapping passbands and helps to improve the number of depth layers compared to RGB color space (see Figures 6(c),6(d)).

3.2. Disparity to Depth Conversion: Single Thin Lens

Let us derive a disparity to depth conversion equation for a single thin lens optical system (Figure 1). For a thin lens (Figure 1(a)), we have:

$$\frac{1}{z_{of}} + \frac{1}{z_{if}} = \frac{1}{f}, \quad (2)$$

where f is the lens focal length, z_{of} the distance between a focused object and the lens, and z_{if} the distance from the lens to the focused image plane. If we move the image sensor towards the lens as shown in Figure 1(b), the image of the object on the sensor is convolved with a color-coded aperture copy which is the circle of confusion, and we obtain:

$$\frac{1}{z_{od}} + \frac{1}{z_{id}} = \frac{1}{f}, \quad (3)$$

$$\frac{1}{z_{of}} + \frac{1+c/D}{z_{id}} = \frac{1}{f}, \quad (4)$$

where z_{id} is the distance from the lens to the defocused image plane, z_{od} is the distance from the lens to the defocused object plane corresponding to z_{id} , c is the circle of confusion diameter and D is the aperture diameter (Figure 1(b)). We can solve this system of equations for the circle of confusion diameter:

$$c = \frac{fD(z_{od} - z_{of})}{z_{od}(z_{of} - f)}, \quad (5)$$

which gives the final result for disparity in pixels:

$$d = \frac{\beta}{2\mu} c = \frac{\beta f D (z_{od} - z_{of})}{2\mu z_{od} (z_{of} - f)}, \quad (6)$$

where μ is the sensor pixel size, $\beta = r_c/R$ is the coded aperture coefficient, $R = D/2$ is the aperture radius, and r_c is the distance between the aperture center and the single channel centroid (Figure 4(b)).

Now we can express the distance between the camera lens and any object only in terms of internal camera parameters and the disparity value corresponding to that object:

$$z_{od} = \frac{bfz_{of}}{bf - 2\mu d(z_{of} - f)}, \quad (7)$$

where $b = \beta D = 2r_c$ is the distance between two centroids, i.e. the color-coded aperture baseline equivalent to the stereo camera baseline. Note that if $d = 0$, z_{od} is naturally equal to z_{of} , i.e. the object is in the camera focus.

3.3. Disparity to Depth Conversion: Complex Lens System

To use (7) in a complex system (objective) we substitute it with a black box with the entrance and exit pupils (see [8] for details) located at the second and the first principal points (H' and H) respectively (see Figure 5).

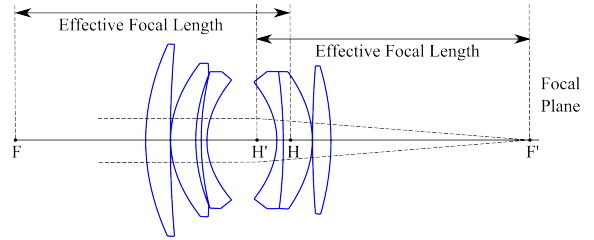


Figure 5. Schematic diagram of the Double Gauss lens used in Canon EF 50mm f/1.8 II lens.

The distance between the entrance and exit pupils and effective focal length are found through a calibration procedure. Since the pupil positions are unknown, we measure the distances to all objects from the camera sensor. Therefore, we modify the disparity to depth conversion equation:

$$\tilde{z}_{od} - \delta = \frac{bf(\tilde{z}_{of} - \delta)}{bf - 2\mu d(\tilde{z}_{of} - \delta - f)}, \quad (8)$$

where \tilde{z}_{od} is the distance between a defocused object and the sensor, \tilde{z}_{of} is the distance between a focused object and the sensor and $\delta = z_{if} + HH'$ is the distance between the sensor and the entrance pupil. Thus, for \tilde{z}_{od} we have:

$$\tilde{z}_{od} = \frac{bf\tilde{z}_{of} - 2\mu d\delta(\tilde{z}_{of} - \delta - f)}{bf - 2\mu d(\tilde{z}_{of} - \delta - f)}, \quad (9)$$

On the right hand side of (9) there are three independent unknown variables, namely \tilde{z}_{of} , b and δ . We discuss their calibration in the next subsection. Other variables are either known or dependent.

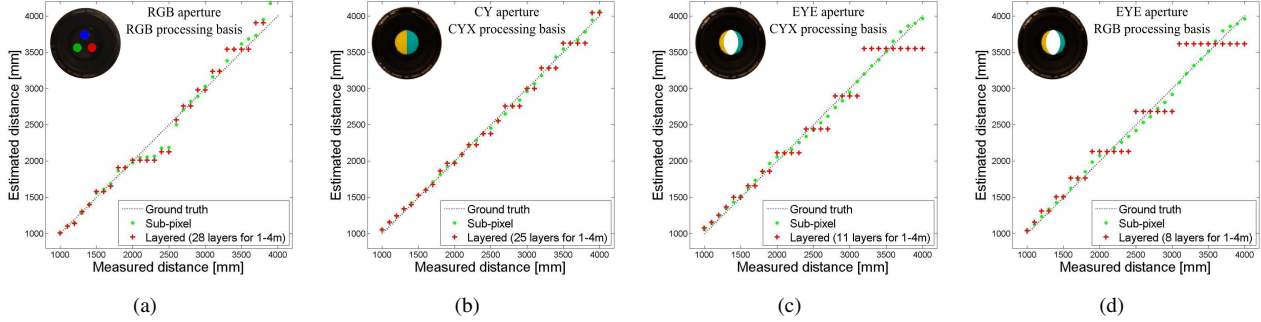


Figure 6. Depth sensor on the axis calibration results for different color-coded aperture designs: (a) three RGB circles processed in RGB color space; (b) cyan and yellow halves coded aperture processed in CYX color space; (c) cyan and yellow coded aperture with opened center processed in CYX color space; (d) cyan and yellow coded aperture with opened center processed in conventional RGB color space.

Another issue arises due to point spread function (PSF) change across the image. This causes a variation in disparity values for objects with the same distances from the sensor but with different positions in the image. A number of researchers encountered the same problem in their work [7, 10, 17, 18]. We perform a specific color-coded aperture depth sensor calibration described in the next subsection to mitigate this effect.

3.4. Depth Sensor Calibration

The first step is the conventional calibration with the pinhole camera model and a chessboard pattern [21]. From this calibration we acquire the distance z_{if} between the sensor and the exit pupil.

To find independent variables \tilde{z}_{of} , b and HH' we capture a set of images of a chessboard pattern moving in a certain range. Each time the object was positioned by hand, that is why small errors are possible (up to 3 mm). The optical system is focused on a certain distance from the sensor. Our experience shows that the error in focusing by hand in a close range is high (up to 20 mm for our lens), so we have to find the accurate value of \tilde{z}_{of} through the calibration.

We extract disparity values and their corresponding distances measured by a ruler on the test scene for all captured images. Now we can find \tilde{z}_{of} and b so that (8) holds with minimal error (RMS error for all measurements).

To account for depth distortion due to optical system *field curvature* we perform the above calibration for all the pixels in the image individually. The resulting color-coded aperture baseline $b(i, j)$ and in-focus surface $\tilde{z}_{of}(i, j)$ are shown in Figures 7(a) and 7(b) respectively.

The procedure described here was implemented on a prototype based on Canon EOS 60D camera and Canon EF 50mm f/1.8 II lens. We captured 31 images where defocused image plane was moving from 1000 mm to 4000 mm with 100 mm steps (z_{od}) and camera was focused on approximately 2000 mm (z_{of}).

The results of our calibration for different coded aperture

designs are presented in Figure 6. Based on the calibration, the effective focal length of our Canon EF 50mm f/1.8 II lens is 51.62 mm, which is in good agreement with the focal length value provided to us by opticians (51.6 mm) who performed an accurate calibration.

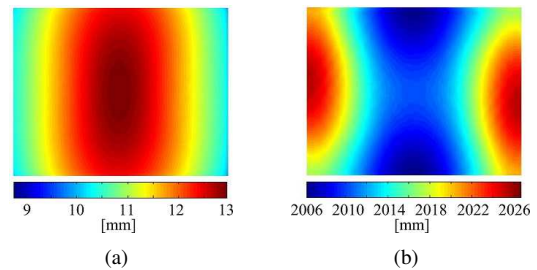


Figure 7. Color-coded aperture depth sensor 3D calibration results: (a) coded aperture equivalent baseline field $b(i, j)$; (b) optical system in-focus surface $\tilde{z}_{of}(i, j)$, where (i, j) are pixel coordinates.

Using the calibration data one can perform an accurate depth map estimation:

$$\tilde{z}_{od}(i, j) = \frac{b(i, j)f\tilde{z}_{of}(i, j) - 2\mu d\delta(\tilde{z}_{of}(i, j) - \delta - f)}{b(i, j)f - 2\mu d(\tilde{z}_{of}(i, j) - \delta - f)}. \quad (10)$$

The floor in Figure 8(a) is flat but appears to be concave on the extracted depth map due to depth distortion (Figure 8(b)). After calibration, the floor surface is corrected and is close to planar (Figure 8(c)). The accuracy of undistorted depth maps extracted with a color-coded aperture depth sensor is sufficient for 3D scene reconstruction as discussed in the next section.

4. Evaluation Results

4.1. Depth Quality

First, let us compare the depth estimation error for layered and sub-pixel approaches. Figure 9 shows that the sub-pixel estimation with the quadratic polynomial interpolation

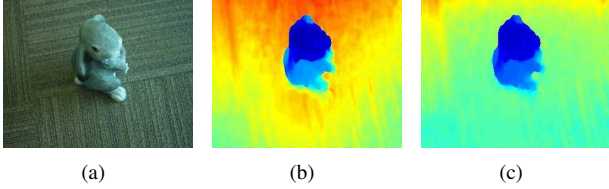


Figure 8. Depth map of a rabbit figure standing on the floor: (a) captured image; (b) distorted depth map, floor appears to be concave; (c) undistorted depth map, floor surface is planar.

significantly improves the depth accuracy.

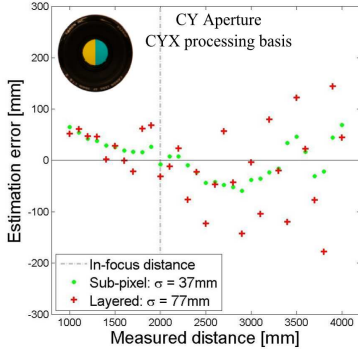


Figure 9. Cyan and yellow coded aperture: depth estimation error comparison for layered and sub-pixel approaches.

Next, we compare the different aperture designs having the same processing algorithm (except aperture corresponding to [5] as it utilizes significantly different approach). Our tests were conducted using Canon EOS 60D DSLR camera with Canon EF 50mm f/1.8 II lens in the same light conditions and for the same distance to the object, while exposure time was adjusted to achieve a meaningful image in each case. Typical results are shown in Figure 10.

We developed a Matlab code for processing. Our non-optimized implementation takes 6 seconds on CPU to extract 1280×1920 raw disparity maps in case of three color filters in the aperture which is very close to [4] implementation (designs I-IV in Figure 10). In case of two color filters in the aperture (designs V,VII in Figure 10) our algorithm takes only 3.5 seconds to extract disparity. Similar disparity estimation algorithm implementation in [5] takes 28 seconds in the same conditions. All tests were performed in single thread mode and with the parameters recommended by their authors.

Raw disparity maps usually require some regularization to avoid strong artifacts. For clarity, we used the same robust regularization method for all extracted results. The variational method [6] was used for global regularization with total variation prior (see the last column in Figure 10). It takes only 3 seconds for 1280×1920 disparity map regularization.

4.2. Color Transparency

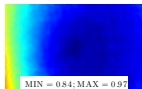
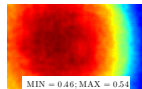
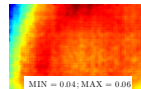
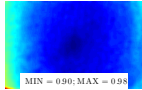
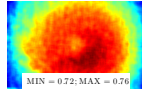
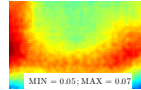
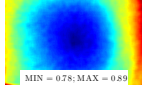
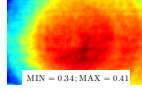
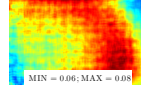
Low light efficiency is a significant drawback of existing coded aperture cameras. We implemented a simple procedure for measuring light efficiency of a coded aperture camera. We capture the first image $I_{i,j}^{nc}$ (here and after (i, j) denote the pixel coordinates) with non-coded aperture and compare it to the second image $I_{i,j}^c$ captured with the same camera presets in the presence of coded aperture. To avoid texture dependency and image sensor noise we use a blurred captured image of a white sheet of paper.

The transparency $T_{i,j}$ shows the fraction of light which passes through the imaging system with coded aperture relative to the same imaging system without coded aperture:

$$T_{i,j} = \frac{I_{i,j}^c}{I_{i,j}^{nc}}. \quad (11)$$

The transparency is different for different colors. We provide the resulting transparency corresponding to colors on image sensors: red, green and blue. In the Table 1 we present the results for a Canon EF 50mm f/1.8 II lens. The integral light efficiency of these designs is 86%, 55%, and 5.5% correspondingly.

Table 1. Transparency maps for different aperture designs corresponding to different image sensor channels

			
Red	 MIN = 0.84; MAX = 0.97	 MIN = 0.46; MAX = 0.54	 MIN = 0.04; MAX = 0.06
Green	 MIN = 0.90; MAX = 0.98	 MIN = 0.72; MAX = 0.76	 MIN = 0.05; MAX = 0.07
Blue	 MIN = 0.78; MAX = 0.89	 MIN = 0.34; MAX = 0.41	 MIN = 0.06; MAX = 0.08

Any imaging system suffers from the vignetting effect which is a reduction of an image brightness at the periphery compared to the image center. Usually, this effect is mitigated numerically. In case of color-coded aperture this restoration procedure should take into account the difference between transparency in different color channels.

4.3. In-focus Image Quality

We conducted experiments for analyzing the in-focus quality of the image captured with the proposed depth sensor using Imatest chart and software [9]. The results are presented in Table 2.

All photos were taken with identical camera settings. It seems that SNR degradation from center to side is induced

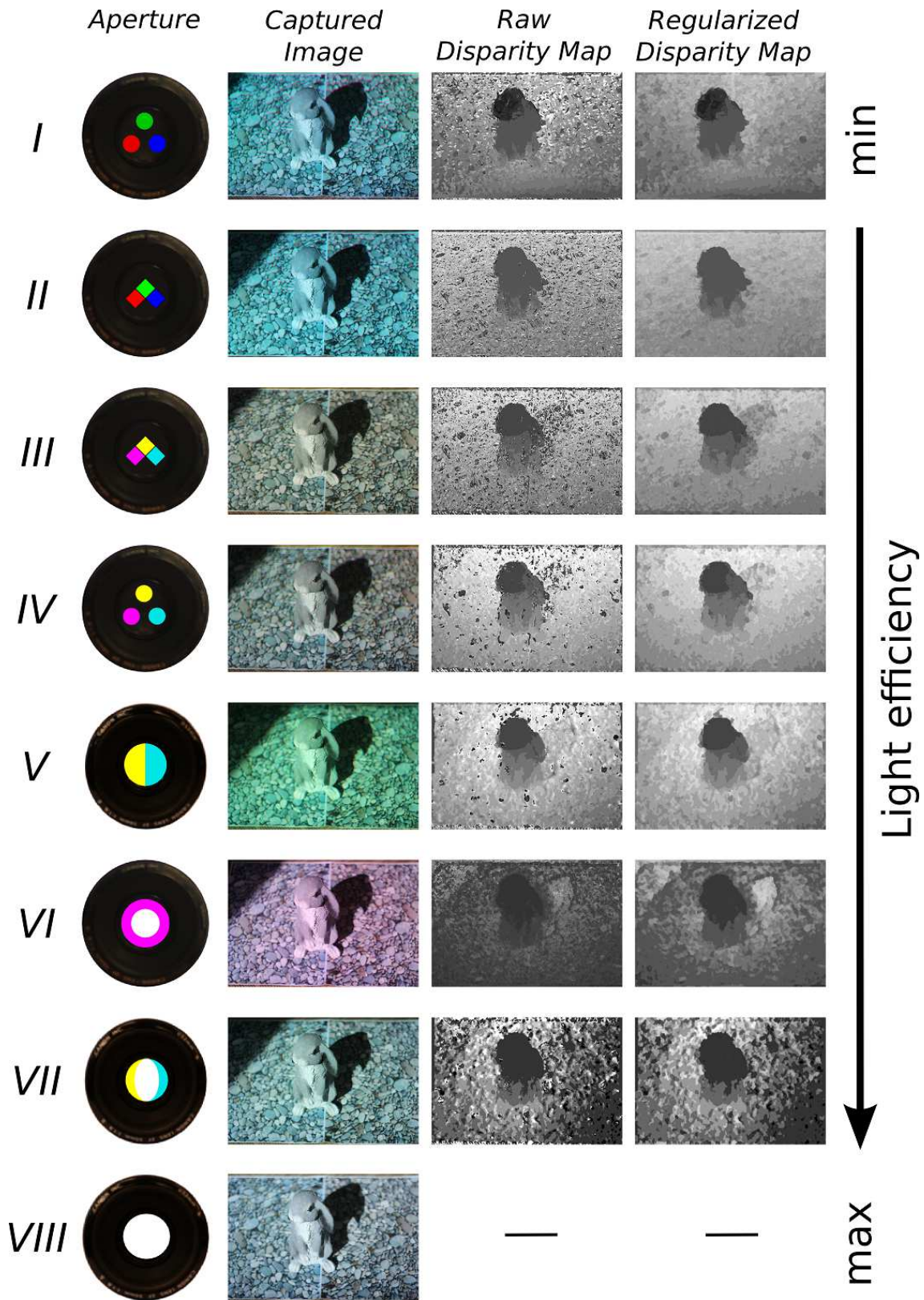


Figure 10. Results comparison with prior art. Rows correspond to different coded aperture designs. From top to bottom: RGB circles [11], RGB squares [4], CMY squares (proposed), CMY circles (proposed), CY halves (proposed), magenta annulus [5], CY with open area (proposed), open aperture. Light efficiency increases from top to bottom (see Figure 11).

Table 2. SNR loss for different apertures in the central and border image areas (dB)

	0.0	0.9	2.3	14.3
central area	0.0	0.9	2.3	14.3
border area	1.5	2.3	3.2	15

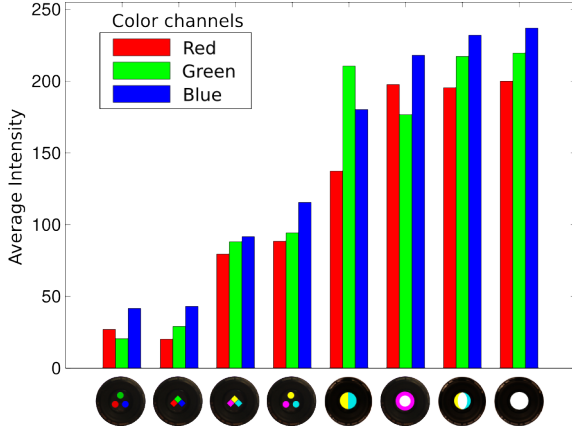


Figure 11. Light efficiency for different coded aperture designs. From left to right: RGB circles [11], RGB squares [4], CMY squares (proposed), CMY circles (proposed), CY halves (proposed), magenta annulus [5], CY with open area (proposed), open aperture.

by lens aberrations. Different apertures provide different SNRs, the value depending on the captured light amount. The loss between aperture 1 and 3 is 2.3 dB. To obtain the original SNR value for aperture 3 one should increase the exposure time by 30%.

4.4. Light Efficiency

It is important to take into account light efficiency while evaluating depth sensor results. We estimated light efficiency via capturing a white sheet of paper through different coded apertures in the same illumination conditions and with the same camera parameters. The light efficiency values are presented for each sensor color channel independently (see Figure 11). The aperture designs are sorted based on their light efficiency.

Apertures V and VI in the Figure 10 have almost same light efficiency but the depth quality of the proposed solution(V) seems to be better. Aperture VII has a higher light efficiency and can be used if depth quality is not an issue.

5. Prototypes and Implementation

A number of prototypes with different color-coded aperture designs were developed based on the Canon EOS 60D DSLR camera and Canon EF 50mm f/1.8 II lens which has

an appropriate f-number and can be easily disassembled [3]. Two examples of captured images and their extracted depth maps are presented in Figures 12(b)-12(e). The corresponding color-coded aperture design is shown in Figure 12(a).

We also targeted two other application scenarios: Image effects based on depth extracted with a smartphone camera; Real-time 3D reconstruction using a handheld or mounted consumer grade camera.

While implementing a smartphone prototype we could not insert the coded aperture into the pupil plane, as most of camera modules cannot be disassembled. However, we disassembled a number of various smartphones and for some models it was possible to insert the color-coded aperture between the front lens of the imaging system and the back cover glass of the camera module (see Figure 13). Unfortunately, we have no access to smartphone imaging system parameters and cannot say how far is this position from the pupil plane.

We implemented an Android application to demonstrate the feasibility of disparity estimation with quality sufficient for depth-based image effects (see Figure 14). Typical running times for different target platforms are summarized in Table 3.

Table 3. Depth extraction time for a single image of HD resolution on different platforms

Platform	Time
Samsung Galaxy S3 (I9300)	30 s
Samsung Note 3 LTE (N9005), OpenCL	5 s
PC CPU (Intel Core i7-2600), Matlab	2 s
PC GPU (Nvidia GeForce 780 Ti), OpenCL	19 ms

5.1. 3D Reconstruction

Our real-time 3D reconstruction scenario is based on a PointGrey Grasshopper 3 digital camera with Fujinon DV3.4x3.8SA-1 lens with embedded Yellow-Cyan color-coded aperture. The PointGrey camera and imaging process are shown in Figures 15(a), 15(b).

We chose the following 3D reconstruction scheme: (1) Get a frame from the camera, and undistort it according to calibration results; (2) Extract the frame depth in millimeters and transform it to a point cloud. Use the color-alignment technique ([4]) to restore color image; (3) Use GPU-accelerated dense tracking and mapping KinFu algorithm (Kinect Fusion algorithm [14]) for camera pose estimation and 3D surface reconstruction.

A PC depth extraction implementation provides 53fps ([15]), OpenCL KinFu provides 45fps ([20]) and the whole 3D reconstruction process works at 15fps which is sufficient for on-the-fly usage.

The test scene and 3D reconstruction results are shown in Figures 15(c)-15(f). Note that a chessboard pattern is not

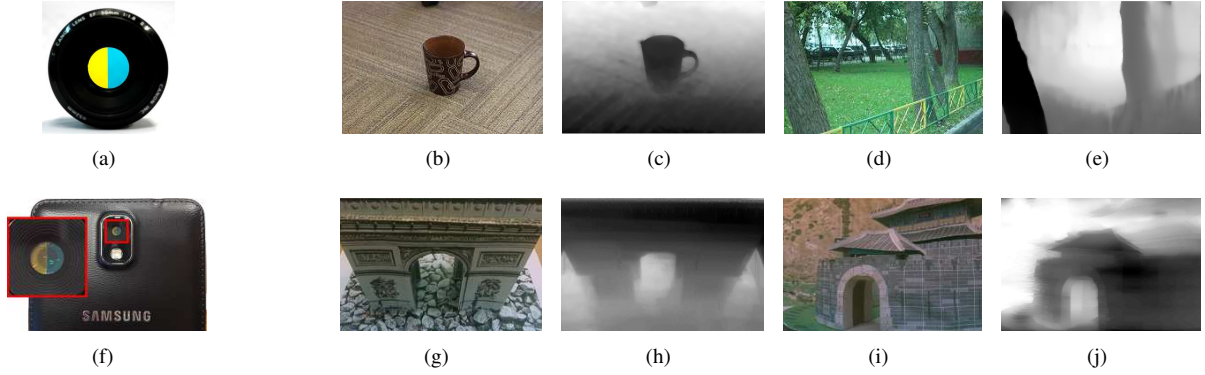


Figure 12. (a) Color-coded aperture inside a DSLR camera lens: (b, d) scenes captured with the DSLR based prototype and (c, e) their corresponding depth maps; (f) color-coded aperture inside a smartphone camera lens: (g, i) tiny models captured with the smartphone based prototype and (h, j) their corresponding disparity maps.



Figure 13. Color-coded aperture smartphone based prototype.

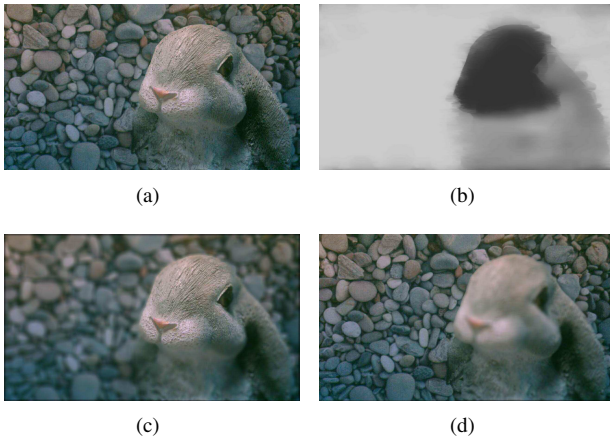


Figure 14. Depth-based image filters: (a) computationally restored image; (b) extracted disparity map; (c) focus on the foreground; (d) focus on the background.

used for tracking but only to provide good texture.

6. Conclusion

In this paper we demonstrated a feasibility of scene 3D reconstruction using single-lens single-frame passive depth

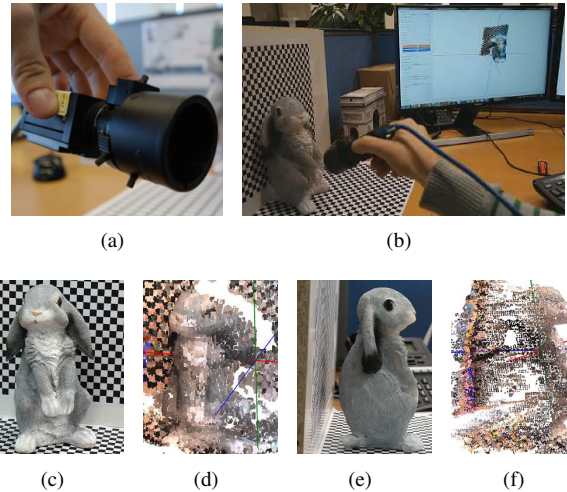


Figure 15. (a) PointGrey Grasshopper 3 camera with color-coded aperture; (b) scene reconstruction process; (c, e) test scene and (d, f) 3D reconstruction results.

sensor based on coded aperture. To the best of our knowledge, this is the first 3D reconstruction for this type of depth sensors. We had to develop a new disparity to depth conversion method as well as a special calibration procedure for color-coded aperture depth sensors.

Moreover, we proposed a light-efficient color-coded aperture designs which make depth extraction practical even with handheld devices. We implemented a number of prototypes and evaluated the performance of different aperture designs.

References

- [1] Y. Amari and E. Adelson. Single-eye range estimation by using displaced apertures with color filters. In *Proc. Int. Conf. Industrial Electronics, Control, Instrumentation and Automation*, pages 1588–1592, 1992. 1, 2

- [2] Y. Bae, H. Manohara, V. White, K. V. Shcheglov, and H. Shahinian. Stereo imaging miniature endoscope. 2011. [1](#)
- [3] Y. Bando. How to disassemble the Canon EF 50mm F/1.8 ii Lens, 2008. <http://web.media.mit.edu/> [1](#), [7](#)
- [4] Y. Bando, B.-Y. Chen, and T. Nishita. Extracting depth and matte using a color-filtered aperture. *ACM Trans. Graph.*, 27(5):134:1–134:9, 2008. [1](#), [2](#), [5](#), [6](#), [7](#)
- [5] A. Chakrabarti and T. Zickler. Depth and deblurring from a spectrally-varying depth-of-field. *Proceedings of the European Conference on Computer Vision*, 2012. [1](#), [5](#), [6](#), [7](#)
- [6] A. Chambolle and T. Pock. A first-order primal-dual algorithm for convex problems with applications to imaging. Master’s thesis, 2010. [5](#)
- [7] D. Dansereau, O. Pizarro, and S. Williams. Decoding, calibration and rectification for lenselet-based plenoptic cameras. In *Proc. CVPR*, pages 1027–1034, June 2013. [2](#), [4](#)
- [8] J. Goodman. *Introduction to Fourier optics*. McGraw-hill, 2008. [3](#)
- [9] Imatest. The SFRplus chart: features and how to photograph it, 2014. [5](#)
- [10] O. Johannsen, C. Heinze, B. Goldluecke, and C. Perwaß. On the calibration of focused plenoptic cameras. In *Time-of-Flight and Depth Imaging. Sensors, Algorithms, and Applications*, pages 302–317. Springer, 2013. [2](#), [4](#)
- [11] E. Lee, W. Kang, S. Kim, and J. Paik. Color shift model-based image enhancement for digital multifocusing based on a multiple color-filter aperture camera. *Consumer Electronics, IEEE Transactions on*, 56(2):317–323, 2010. [1](#), [2](#), [6](#), [7](#)
- [12] S. Lee, N. Kim, K. Jung, M. H. Hayes, and J. Paik. Single image-based depth estimation using dual off-axis color filtered aperture camera. In *Acoustics, Speech and Signal Processing (ICASSP), 2013 IEEE International Conference on*, pages 2247–2251. IEEE, 2013. [1](#), [2](#)
- [13] A. Levin, R. Fergus, F. Durand, and W. T. Freeman. Image and depth from a conventional camera with a coded aperture. *ACM Trans. Graph.*, 26(3), July 2007. [1](#)
- [14] R. A. Newcombe, S. Izadi, and E. AL. Kinectfusion: Real-time dense surface mapping and tracking. In *Mixed and augmented reality (ISMAR), 2011 10th IEEE international symposium on*, pages 127–136. IEEE, 2011. [7](#)
- [15] I. Panchenko and V. Bucha. Hardware accelerator of convolution with exponential function for image processing applications. In *Seventh International Conference on Graphic and Image Processing*, pages 98170A–98170A. International Society for Optics and Photonics, 2015. [7](#)
- [16] I. Panchenko, V. Paramonov, and V. Bucha. Depth estimation algorithm for color coded aperture camera. In *Electronic Imaging 2016: 3D Image Processing, Measurement (3DIPM), and Applications*. To appear. IS&T, 2016. [2](#), [3](#)
- [17] P. Trouvé, F. Champagnat, G. Le Besnerais, G. Druart, and J. Idier. Design of a chromatic 3d camera with an end-to-end performance model approach. In *Computer Vision and Pattern Recognition Workshops (CVPRW), 2013 IEEE Conference on*, pages 953–960. IEEE, 2013. [2](#), [4](#)
- [18] P. Trouvé, F. Champagnat, G. Le Besnerais, J. Sabater, T. Avignon, and J. Idier. Passive depth estimation using chromatic aberration and a depth from defocus approach. *Applied optics*, 52(29):7152–7164, 2013. [2](#), [4](#)
- [19] A. Veeraraghavan, R. Raskar, A. Agrawal, A. Mohan, and J. Tumblin. Dappled photography: Mask enhanced cameras for heterodyned light fields and coded aperture refocusing. *ACM Trans. Graph.*, 26(3):69:1–69:12, 2007. [1](#)
- [20] S. Zagoruyko and V. Chernov. Fast depth map fusion using OpenCL. In *Conference on Low Cost 3D (LC3D)*, 2014. [7](#)
- [21] Z. Zhang. A flexible new technique for camera calibration. *IEEE Trans. PAMI*, 22(11):1330–1334, 2000. [4](#)
- [22] C. Zhou, S. Lin, and S. K. Nayar. Coded aperture pairs for depth from defocus and defocus deblurring. *International journal of computer vision*, 93(1):53–72, 2011. [1](#)